Journal of Molecular Spectroscopy 280 (2012) 68–76

Contents lists available at SciVerse ScienceDirect

Journal of Molecular Spectroscopy

journal homepage: www.elsevier.com/locate/jms

A K_a-band chirped-pulse Fourier transform microwave spectrometer

Daniel P. Zaleski [a], Justin L. Neill [a], Matt T. Muckle [a], Nathan A. Seifert [a], P. Brandon Carroll [b], Susanna L. Widicus Weaver [b,*], Brooks H. Pate [a,*]

[a] Department of Chemistry, University of Virginia, McCormick Rd., Charlottesville, VA 22904, USA
[b] Department of Chemistry, Emory University, 1515 Dickey Drive, Atlanta, GA 3032, USA

ARTICLE INFO

Article history:
Available online 14 August 2012

Keywords:
Broadband spectroscopy
Microwave spectroscopy
Acetaldehyde
Ethyl formate

ABSTRACT

The design and performance of a new chirped-pulse Fourier transform microwave (CP-FTMW) spectrometer operating from 25 to 40 GHz (K_a-band) is presented. This spectrometer is well-suited for the study of complex organic molecules of astronomical interest in the size range of 6–10 atoms that have strong rotational transitions in K_a-band under pulsed jet sample conditions (T_{rot} = 1–10 K). The spectrometer permits acquisition of the full spectral band in a single data acquisition event. Sensitivity is enhanced by using two pulsed jet sources and acquiring 10 broadband measurements for each sample injection cycle. The spectrometer performance is benchmarked by measuring the pure rotational spectrum of several isotopologues of acetaldehyde in natural abundance. The rotational spectra of the singly substituted ^{13}C and ^{18}O isotopologues of the two lowest energy conformers of ethyl formate have been analyzed and the resulting substitution structures for these conformers are compared to electronic structure theory calculations.

1. Introduction

Chirped-pulse Fourier transform microwave (CP-FTMW) spectrometers provide instantaneous broadband spectral coverage for measurement of molecular rotational spectra [1]. The sensitivity of the spectrometer can be enhanced by using multiple pulsed jet sources to increase the number of molecules in the active volume and by acquiring multiple spectra for each sample injection cycle. These broadband spectrometers offer complementary performance to narrowband cavity FTMW spectrometers – based on the Balle–Flygare design [2]. The CP-FTMW design is best suited for applications that require a survey spectrum of a sample with an unknown composition. The mixture can include a variety of distinct chemical species or several isomers (conformational or isotopologues) of a single species. In these applications, the key advantages of CP-FTMW spectrometers are accurate relative intensities across the measurement band, shorter measurement time in acquiring a broad-bandwidth spectrum (in part from the simplified operation requiring no mechanical repositioning of cavity mirrors), and the ability to use multiple pulsed jet sources in the free space interaction region to minimize sample consumption and measurement time to reach a target sensitivity. In contrast, the passive gains inside the microwave cavity achieved in Balle–Flygare spectrometers are better suited for applications where a single transition is monitored since optimal excitation conditions can routinely be achieved with the power available from standard microwave components. The passive gain may also give an advantage to Balle–Flygare spectrometers for studies of molecules with small dipole moments and may be particularly important in the K_a-band frequency region that is the focus of this work because the microwave power amplifiers required for CP-FTMW spectroscopy provide relatively low power (about 40 W compared to 300 W or more for frequencies below 18 GHz). The cavity FTMW spectrometers are also well suited to limited search applications where an accurate prediction of the spectrum for the species of interest is available. During the past few years, the applications of chirped-pulse spectroscopy have been numerous, including the study of metal-containing molecules [3–6], conformationally rich molecules [7], and molecular clusters [8]. Chirped-pulse instruments have also been developed to work over reduced bandwidths and at low frequency [9,10].

Recently, the CP-FTMW technique has been extended to mm-wave operation. The Field group at MIT has constructed a chirped-pulse millimeter-wave spectrometer (CP-mmW) operating between 70–84 GHz and 87–102 GHz and applied it to studies of molecules produced in electric discharge sources [11] and the spectroscopy of atomic Rydberg states prepared by laser [12]. The operation of CP-FT spectrometers at frequencies up to about 1 THz has been demonstrated at NIST [13]. Both of these high-frequency spectrometers have used solid-state frequency multiplier devices to generate the chirped-excitation pulse. Despite the relatively low peak powers of these sources (<100 mW) both of

* Corresponding authors.
E-mail addresses: susanna.widicus.weaver@emory.edu (S.L. Widicus Weaver), bp2k@virginia.edu (B.H. Pate).

0022-2852/$ - see front matter © 2012 Elsevier Inc. All rights reserved.
http://dx.doi.org/10.1016/j.jms.2012.07.014

these spectrometers have demonstrated high measurement sensitivity.

The extension of CP-FTMW techniques to mm-wave and THz frequency ranges is expected to impact spectroscopic studies of molecules with astrochemical importance. A new generation of radio astronomy interferometers that combine broadband spectral detection with high spatial resolution have commenced science operations in the past 2 years. The Jansky Very Large Array (JVLA) operates in the microwave frequency range (up to 50 GHz), and the Atacama Large Millimeter/Sub-millimeter Array (ALMA) has the potential for mm-wave spectral coverage in all atmospheric windows up to 1 THz. These facilities will produce about 1 PB/yr of spatially-resolved high-resolution interstellar molecular rotational spectra. Science verification data demonstrating the capabilities of ALMA have recently been made publicly available [14]. With the improved detection sensitivity and spatial resolution of next generation radio astronomy observatories, it is reasonable to expect that the amount of unassigned astronomical spectral data will increase rapidly. For a typical astronomical survey [15], there are already more unassigned transitions than known transitions. Since the rotational spectra of most readily available molecules are known, the remaining unknown transitions are likely novel species including high energy isomers, molecular ions, radicals, and vibrationally excited states that are populated in the hot core star-forming regions of interstellar clouds, where the organic chemistry becomes complex. CP-FTMW spectrometers are compatible with pulsed molecular beam sources, like electric discharge sources, that are capable of producing short-lived non-terrestrial species (e.g. ions, radicals, and high energy isomers) in sufficient quantities for spectroscopic analysis [16–21]. In particular, the combination of high spectral resolution, measurement dynamic range, and rotational cooling of pulsed jet spectrometers for rotational spectroscopy facilitate the analysis of the complex sample mixtures produced by reactive chemistry sources.

Here we demonstrate the operation of a K_a-band (26–40 GHz) CP-FTMW spectrometer. The spectrometer design is based on previous spectrometers operating below 18 GHz [1] and uses a pulsed traveling wave tube amplifier to achieve efficient sample excitation. This frequency range is well-suited to the study of molecules of astrochemical interest, typically containing 7 or fewer non-hydrogen atoms, because the peak intensity of their rotational spectra often fall in the K_a-band frequency range under molecular beam conditions (T_{rot} = 1–10 K). This instrument builds on technological advances in arbitrary waveform generation that is commonly used for telecommunications. Such an instrument will help unite laboratory spectroscopy with radio astronomical measurements and, in particular, provides direct spectral overlap with the National Radio Astronomy Observatory Green Bank Telescope (GBT) and JVLA. This new spectrometer facilitates the study of molecules relevant to astrochemistry with the spectral simplification of a pulsed-jet source.

2. Experimental

A schematic of the K_a-band CP-FTMW spectrometer is shown in Fig. 1. A 24 GS/s arbitrary waveform generator (AWG) (Tektronix AWG7122B) creates a 1 μs linear frequency sweep (chirped pulse) covering the frequency range from 10.5 to 3 GHz. A 12.2 GHz low-pass filter is used on the output of the AWG to filter out high frequency components that are produced by the mixing of the primary sweep with the AWG clock frequency. The chirped pulse is up-converted using a triple-balanced mixer (Miteq TB0440LW1) and a 23 GHz local oscillator (Microwave Dynamics, PLO-4070-23.00). This local oscillator is a 23 GHz phase-locked dielectric oscillator (PDRO) that has its output filtered by a 6-pole cavity bandpass filter (K&L Microwave, 6C62-23000/T100-K/K) to

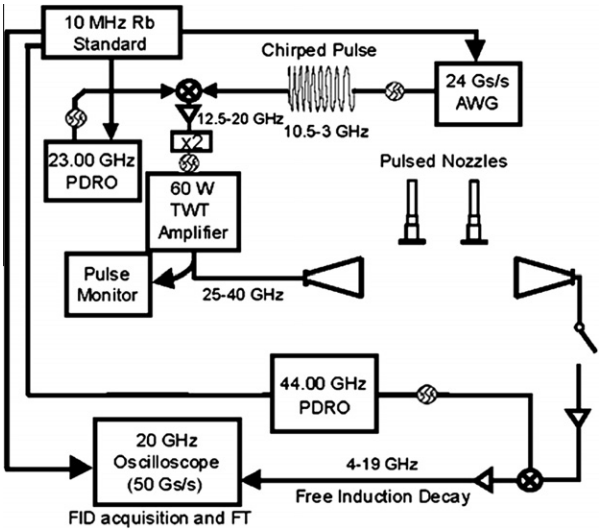

Fig. 1. Schematic of the K_a-band CP-FTMW spectrometer.

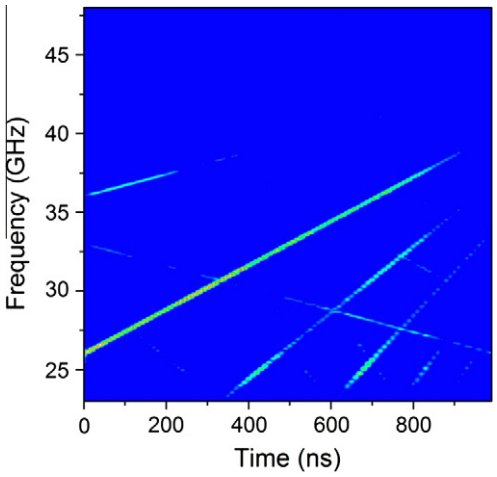

Fig. 2. A spectrogram of the microwave pulse before entering the TWTA. The effects of sub-harmonic mixing and additional outputs of the doubler can be seen.

improve spectral purity. The lower frequency sideband from this mixing stage, with a frequency range of 12.5–20 GHz, is used to generate the final chirped-pulse after frequency doubling. In this design, the active frequency doubler (Wright Technologies, 100 mW output power, ATX40-220) accepts input frequencies from about 13–20 GHz with a sharp fall off in doubling efficiency above 20 GHz input frequency. Therefore, this device also serves to filter out the upper sideband of the mixing stage (26–33.5 GHz). The microwave pulse is amplified (Miteq, JS4-12002600-25-5P, 12–26 GHz bandwidth) to 10 mW prior to being input to the active frequency doubler. The frequency-doubled output is filtered by a nominal 26–40 GHz bandpass filter (Microwave Circuits, Inc., H26G40G1) and attenuated to 1 mW peak power for input to the K_a-band power amplifier. Fig. 2 shows a spectrogram of the chirped pulse at this stage. In addition to the primary pulse, spurious chirps due to sub-harmonic mixing are observed and are approximately 20 dB weaker than the primary chirp.

The K_a-band chirped pulse is input into a pulsed traveling wave tube amplifier (TWTA, Applied Systems Engineering, 187Ka 105304-1) which has a measured output of 60 W mid-band with power output of greater than 40 W across K_a-band. This amplifier

and the overall microwave pulse generation circuit provide useful pulse output power down to about 25 GHz giving a small extension of the frequency range of the spectrometer over the usual specification of 26–40 GHz for K_a-band. The amplified microwave pulse is coupled into and out of the vacuum chamber by WR-28 rectangular waveguide bulkhead feedthroughs with Kapton pressure windows used to maintain vacuum. The microwave pulse is broadcasted and received using 24 dBi gain microwave horn antennas (Advanced Technical Materials, PNR 28-449-6/24). The horn antennas are spaced by 60 cm and can accommodate two pulsed nozzles (1 mm nozzle diameter, General Valve Series 9) oriented perpendicular to the axis of microwave propagation. The two nozzles are spaced by 20 cm to prevent interference between the supersonic molecular beam expansions.

The receiver is protected from the high-power TWTA pulse by a SPST switch (Millitech, PSP-28-SIASF). The molecular free induction decay (FID) signals are amplified by a low-noise high gain amplifier (Miteq, 37 dB gain, 3 dB noise figure, JS42-26004000-38-5P), then downconverted using a triple-balanced mixer (Miteq, TB0440LW1) with a 44 GHz PDRO (Microwave Dynamics, PLO-4070-44.00), filtered by a bandpass filter (Eastern Wireless TeleComm, EWT-31-0272), as the local oscillator. The downconverted FID signals (4–19 GHz) are amplified by a second 20 dB gain amplifier (Miteq, AMF-3D-020265-60-10P) and subsequently digitized by a 50 GS/s oscilloscope (Tektronix DPO72004). A 10 MHz rubidium standard is used to phase-lock all frequency sources to permit time-domain signal averaging. On each valve injection cycle, 10 microwave pulses are applied, separated by 20 μs, and 10 FIDs are detected, each with a duration of 10 μs. The frequency domain spectrum is obtained from fast Fourier transform of the time-domain FID and reported as the magnitude spectrum. The spectra presented here are the average of at least 300 000 molecular FIDs, and have a transition FWHM linewidth of approximately 200 kHz after the application of a Kaiser–Bessel digital filter [1]. Spectral analysis was carried out using the AABS software package [22,23] in tandem with SPFIT/SPCAT [24,25]. Electronic structure theory calculations were carried out using the Gaussian09 software package [26].

Below we present the spectra of three molecules: carbonyl sulfide (OCS), acetaldehyde, and ethyl formate. All samples were purchased from Aldrich and used without further purification. The OCS and ethyl formate gas samples were 0.2% mixtures in neon while acetaldehyde was diluted to 0.1% due to its higher propensity to complex in the supersonic expansion. Each spectrum was collected using a backing pressure of approximately 1 atm.

3. Results

3.1. OCS

We demonstrate the sensitivity and relative intensity accuracy of the K_a-band CP-FTMW spectrometer using OCS due to its large number of isotopologues that can be observed in natural abundance. The spectrum of the $J = 3–2$ transitions of OCS and its isotopologues is shown in Fig. 3, where the signal-to-noise ratio of the normal species transition is approximately 170 000:1 after 400 000 signal averages (14 h of data collection). The weakest isotope detected is the $^{18}O^{13}C^{32}S$ isotopologue, with a natural abundance of 0.00211% (44 000 times less abundant than the $^{16}O^{12}C^{32}S$ species). There are few high-frequency resolution measurements (uncertainty of 5 kHz or better) for the transitions of the minor isotopologues available in the literature. We present the predicted frequencies of these isotopologues from the CDMS catalog [28], which have quoted uncertainties of 2.5 kHz or better, but are not experimentally measured values. Agreement between the CP-FTMW frequencies and these tabulated values are better than 10 kHz.

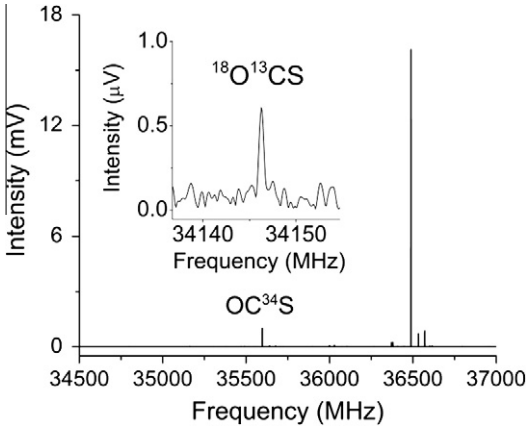

Fig. 3. The signals for the $J = 3–2$ rotational transition of OCS (0.2% OCS in neon). The inset shows an expanded view of the $^{18}O^{13}CS$ isotopologue (0.00211% natural abundance) transition.

In Table 1 we also give the relative intensity accuracy of the spectrometer across a large dynamic range. The literature isotope abundances are compared to the relative intensity measurements in the CP-FTMW spectrum. In this determination, we neglect the small differences between the dipole moments of the various isotopologues. We find that the transition intensities are accurate within 30%, somewhat higher than but comparable to the value determined from a similar analysis in the 6.5–18.5 GHz CP-FTMW instrument [1].

We have also tested the sweep bandwidth dependence of the OCS transition intensity. The result of this study is shown in Fig. 4. The duration of the chirped pulse was kept constant at 1 μs. As in the 6.5–18.5 GHz CP-FTMW instrument, the signal is found to vary with $\alpha^{-1/2}$ except at very low bandwidths (where the measurement is no longer in the weak pulse limit). A more powerful 140 W TWTA [29] is available from Applied Systems Engineering, but at a premium in cost. The major limitation in extending this system beyond 40 GHz is the limited availability of high power, high frequency radiation sources.

3.2. Acetaldehyde

Acetaldehyde is one of the simplest and most thoroughly studied molecules that exhibits spectral features arising from the internal motion of a single methyl rotor, and is an excellent test case for high-barrier internal rotation [30]. Its isotopologues, including the various deuterated species, have also been well-studied in the centimeter, millimeter, and submillimeter ranges [31–37]. Because of the abundance of previous work on this molecule, this is an excellent system for benchmarking the spectrometer.

Acetaldehyde is also a well-known interstellar molecule. It has been detected in various source types, including translucent clouds, cold molecular clouds, and hot cores, with reported detections in Sgr B2, L134N, TMC-1, the Orion Compact Ridge, and CB17, among others [38–46]. Acetaldehyde is proposed to form from both photodissociation-driven radical–radical reactions on grain surfaces and ion-neutral gas-phase reactions [47], and the observed isotopic ratios should depend strongly on these formation pathways. Detection and determination of the abundances of the various isotopic species of acetaldehyde in interstellar sources could provide valuable constraints on chemical models, and could help elucidate the importance of acetaldehyde's various possible formation pathways.

Here we present re-measured frequencies previously reported by Kilb et al., Turner et al. [37,33], and Martinache and Bauder to

Table 1
A comparison of the measured rotational transitions of OCS ($J = 3–2$) and natural abundances as measured by the K_a-band CP-FTMW spectrometer to that of the NIST-FTMW cavity and calculated values from CDMS. Intensities resulting from chirped-pulse excitation, on average, vary from the literature values by 30%. If $O^{13}C^{33}S$ 3/2–1/2 is not included, the average intensity variance drops to 25%.

Isotopologue	$F' \leftarrow F''$	CP freq. (MHz)	Lit. freq. (MHz)	Measured relative signal	Lit. nat. abund. (%)	% Diff.
OCS		36488.802	36488.813(2)[a]	–	93.74	–
$OC^{34}S$		35596.862	35596.91(30)[a]	5.300	4.158	27.46
$O^{13}CS$		36371.392	36371.390(30)[a]	1.332	1.053	26.54
$OC^{33}S$						
	7/2–7/2	36022.414	36022.424[b]	0.0411	0.0305	35.05
	5/2–3/2[c]	6027.896	36027.902[b]	0.1593	0.11899	33.92
	3/2–1/2[c]	–	36027.902[b]	–	0.07437	–
	7/2–5/2c	–	36029.707[b]	–	0.1821	–
	9/2–7/2[c]	36029.700	36029.707[b]	0.3691	0.26559	38.99
	5/2–5/2	36033.090	36033.102[b]	0.0337	0.03885	13.13
	3/2–3/2	36035.172	36035.179[b]	0.0337	0.02974	13.47
^{18}OCS		34229.016	34229.045(30)[a]	0.2597	0.188	38.15
$O^{13}C^{34}S$		35470.258	35470.264(20)[a]	0.0451	0.0467	−3.94
^{17}OCS		35301.924	35301.90[b]	0.0214	0.035	−38.80
$OC^{36}S$		34798.026	34798.022[b]	0.0163	0.0167	−4.10
$^{18}OC^{34}S$		33359.698	33359.69[b]	0.0105	0.00834	32.16
$O^{13}C^{33}S$						
	3/2–1/2	35905.786	35905.78[b]	0.0021	0.00107	101.37
	9/2–7/2	35907.594	35905.586[b]	0.0026	0.00253	5.74
$^{18}O^{13}CS$		34146.282	34146.273[b]	0.0021	0.0034	41.10

[a] [27].
[b] [28].
[c] For $OC^{33}S$, the $F = 5/2–3/2$ and the 3/2–1/2 transitions are blended at the experimental resolution, as well as the $F = 7/2–5/2$ and 9/2–7/2 transitions.

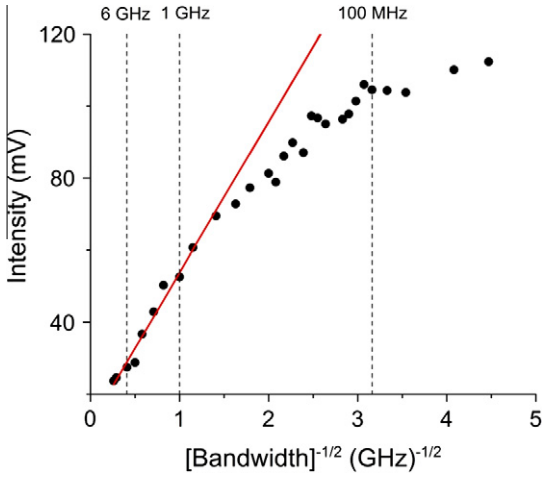

Fig. 4. The efficiency of the K_a-band CP-FTMW spectrometer for creating the molecular polarization for the $J = 3–2$ rotational transition of OCS. Intensities were recorded after 100 signal acquisitions. The red line shows the weak pulse limit. For convenience, dashed lines have been provided at the bandwidths of 6 GHz, 1 GHz, and 100 MHz (left to right). (For interpretation of the references to color in this figure legend, the reader is referred to the web version of this article.)

higher precision and in natural abundance. At higher frequencies the mm/sub-millimeter wave spectrum of the normal species of acetaldehyde has also already been reported by Barclay et al. from 230 to 325 GHz [48]. The ^{13}C isotopic species has also been studied up to 950 GHz [49]. The deuterated species CD_3CHO [31] and CH_3CDO [50] have also been recorded at mm/sub-millimeter wave frequencies.

The signal-to-noise ratio of the strongest line in the 25–40 GHz spectrum, the $2_{02}–1_{01}$ transition pair of CH_3CHO, is approximately 100 000:1 after 700 000 signal averages (25 h of data collection). We detect transitions of seven isotopologues of acetaldehyde, six singly-substituted isotopologues ($^{13}CH_3CHO$, $CH_3{}^{13}CHO$, $CH_3CH^{18}O$, *sym*-CH_2DCHO, *asym*-CH_2DCHO, and CH_3CDO) as well as $^{13}CH_3{}^{13}CHO$. The observed transition frequencies, compared to the frequencies of previous studies, are presented in Tables 2–5. We have included new measurements of the $1_{01}–0_{00}$ isotopologue transitions, measured using the 6.5–18.5 GHz CP-FTMW spectrometer. The frequencies are in good agreement for all species, with the exception of the $2_{02}–1_{01}$ (A) transition of the $^{13}CH_3CHO$

Table 2
Rotational transition frequencies for $^{13}CH_3CHO$, $CH_3{}^{13}CHO$, and $CH_3CH^{18}O$.

Species	Transition	CP-FTMW frequency (MHz)	Kilb et al. [36] frequency (MHz)
$^{13}CH_3CHO$	$1_{01}–0_{00}$ E	18703.5560	18703.69
	$1_{01}–0_{00}$ A	18706.2978	18706.46
	$2_{12}–1_{11}$ A	36402.8397	36402.86
	$2_{12}–1_{11}$ E	36628.0260	36628.12
	$2_{02}–1_{01}$ E	37390.7509	37391.12
	$2_{02}–1_{01}$ A	37396.7760	37393.36
	$2_{11}–1_{10}$ E	38186.9974	38186.94
	$2_{11}–1_{10}$ A	38420.3615	38420.36
$CH_3{}^{13}CHO$	$1_{01}–0_{00}$ E	19229.5551	19229.94
	$1_{01}–0_{00}$ A	19232.4161	19232.43
	$2_{12}–1_{11}$ A	37370.6522	37370.90
	$2_{12}–1_{11}$ E	37574.5253	37574.60
	$2_{02}–1_{01}$ E	38439.4350	38439.56
	$2_{02}–1_{01}$ A	38445.2286	38445.38
	$2_{11}–1_{10}$ E	39343.7567	39343.40
	$2_{11}–1_{10}$ A	39557.0221	39557.00
$CH_3CH^{18}O$	$1_{01}–0_{00}$ E	18367.6481	18367.75
	$1_{01}–0_{00}$ A	18370.3899	18370.23
	$2_{12}–1_{11}$ A	35754.6034	–
	$2_{12}–1_{11}$ E	–[a]	–
	$2_{02}–1_{01}$ E	36719.6540	36719.90
	$2_{02}–1_{01}$ A	36725.1377	36725.26
	$2_{11}–1_{10}$ E	–[a]	–
	$2_{11}–1_{10}$ A	37725.0614	37724.40
$^{13}CH_3{}^{13}CHO$	$1_{01}–0_{00}$ E	18669.5575	18670.03
	$1_{01}–0_{00}$ A	18672.1563	18672.02
	$2_{02}–1_{01}$ E	37321.4664	37322.20
	$2_{02}–1_{01}$ A	37326.7832	37326.98
	$2_{11}–1_{11}$ E	–	38164.50
	$2_{11}–1_{11}$ A	38378.8767	38378.82

[a] The predicted frequencies for these transitions fall in regions of spurious modulations resulting from overdriving the mixer, and are therefore not reported.

Table 3
Rotational transition frequencies for *sym*-CH_2DCHO.

Species	Transition	CP-FTMW frequency (MHz)	Turner et al. [37] frequency (MHz)
CH_2DCHO	1_{01}–0_{00}	18501.7585	18501.80
	2_{12}–1_{11}	35775.5842	35775.66
	2_{02}–1_{01}	–[a]	36974.41
	2_{11}–1_{10}	38231.0572	38231.02

[a] There is a line observed at 36974.5712 MHz that is about a factor of 5 too strong for deuterium in natural abundance.

Table 4
Rotational transition frequencies for *asym*-CH_2DCHO.

Species	Transition	CP-FTMW frequency (MHz)	Turner et al. [33] frequency (MHz)
CH_2DCHO	1_{01}–0_{00} 0_-	18000.7723	18000.80
	1_{01}–0_{00} 0_+	18001.7471	18001.75
	2_{12}–1_{11} 0_-	34757.4692	34757.49
	2_{12}–1_{11} 0_+	35205.0247	35205.05
	2_{12} (−)–1_{10} (+)	35320.7531	35320.80
	2_{02}–1_{01} 0_-	35989.6603	35989.67
	2_{02}–1_{01} 0_+	35991.6153	35991.63
	2_{11}–1_{10} 0_-	36798.1138	36798.13
	2_{11} (+)–1_{11} (−)	36685.1311	36685.10
	2_{11}–1_{10} 0_+	–	37248.40

Table 5
Rotational transition frequencies for CH_3CDO.

Species	Transition	CP-FTMW frequency (MHz)	Martinache and Bauder [32] frequency (MHz)
CH_3CDO	1_{01}–0_{00} E	18889.8086	18889.870
	1_{01}–0_{00} A	18891.9067	18891.686
	1_{10}–1_{01} E	36313.5996	36313.516
	2_{12}–1_{11} A	36354.0354	36354.093
	1_{10}–1_{01} A	36403.3632	36403.015
	2_{12}–1_{11} E	–[a]	36413.426
	2_{02}–1_{01} E	37736.5055	37736.560
	2_{02}–1_{01} A	37740.2010	37740.282
	2_{11}–2_{02} E	–[a]	–
	2_{11}–2_{02} A	37874.2161	37874.322
	2_{11}–1_{10} E	39145.8969	39146.128
	2_{11}–1_{10} A	39211.7958	39211.479

[a] See Table 2 for superscript.

isotopologue, which is in disagreement by 3 MHz, as shown in Fig. 5. We attribute this deviation to a typographical error in the previous work, as the Hamiltonian model presented in this report predicts a transition frequency near to that observed in the CP-FTMW spectrometer.

3.3. Ethyl formate

The two lowest-energy conformers of ethyl formate are referred to in the literature as *trans* (or *anti*) and *gauche*, which refers to the orientation of the ethyl group; both isomers are *cis* in the ester dihedral. Fig. 6 shows the calculated one-dimensional relaxed conformational potential energy surface from electronic structure theory (MP2/6-311++G(d,p)). The rotational spectra of both of these conformers have been studied in the centimeter [51–53] and millimeter/submillimeter [54,55] frequency ranges. The lowest-energy *cis–trans* conformer (where we identify the conformers by their orientation about the ester bond, followed by the stereochemistry of the ethyl group) was recently detected in the Sagittarius B2(N) hot core [56]. However, to our knowledge, there have to date been no reports of the rotational spectra of any isotopologues of this species.

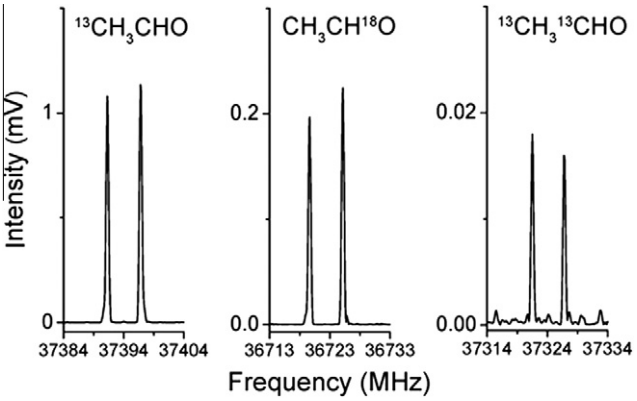

Fig. 5. Three separate magnifications showing the 2_{02}–1_{01} rotational transition of some isotopes of acetaldehyde measured in natural abundance. The two peaks are due to internal rotation of the methyl group.

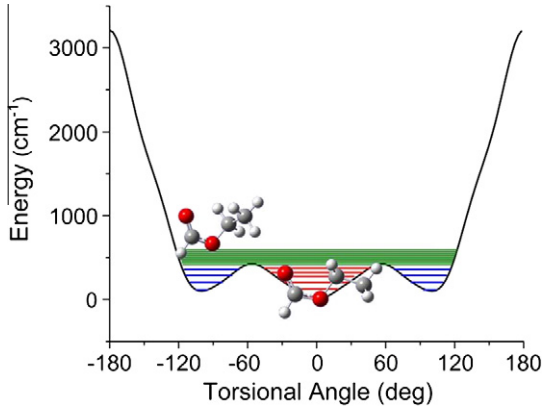

Fig. 6. The torsional potential (C—O—C—C) of ethyl formate is shown. The torsional energy levels up to about 700 cm^{-1} calculated from this 1D potential are shown. The equilibrium geometries of the two conformational minima (*cis–trans* and *cis–gauche*) are also shown. Calculations were performed at the MP2/6-311++G(d,p) level of theory.

The experimental CP-FTMW spectrum of ethyl formate is shown in Fig. 7. We have measured this spectrum with both the 6.5–18.5 GHz and 25–40 GHz spectrometer configurations, with a total of 300 000 FIDs collected in each configuration. From these spectra the rotational spectra of each of the singly substituted ^{13}C and ^{18}O isotopologues of both the *cis–trans* and *cis–gauche* conformers were measured and fit to determine the rotational constants of each isotopologue. The distortion constants for each isotopologue were held fixed to their values for the normal species.

These rotational constants were then used to determine the position of each heavy atom in the molecular principal axis system, using Kraitchman's equations as implemented in the KRA program [23] to determine the r_s structure of the backbone of these two conformers. For the *cis–trans* isomer, due to its C_s symmetry, each of the heavy atoms is located in the *a–b* plane, so the value of the *c* coordinate was fixed to zero. The backbone of the *cis–gauche* conformer is non-planar, and so this constraint was not imposed.

The substitution structures, overlaid with the equilibrium geometry ab initio structures calculated at an MP2/6-311++G(d,p) level, are presented in Fig. 8, showing good agreement between the experimentally derived and theoretical structures. The atom positions and internal coordinates of the two conformers, derived using

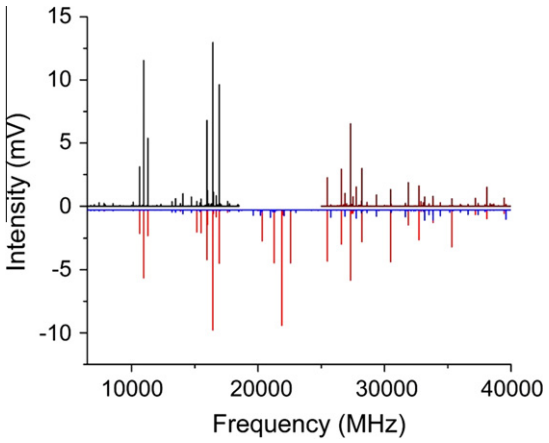

Fig. 7. Broadband experimental spectra of ethyl formate acquired from 6.5 to 18.5 GHz (black) and 25 to 40 GHz (dark red). Shown with negative intensity are simulations of the *cis–trans* (red) and *cis–gauche* (blue) isomers of ethyl formate at 1.5 K (rotational temperature). The two spectra have been scaled for noise level, showing that despite having less power, the sensitivity is still similar. (For interpretation of the references to color in this figure legend, the reader is referred to the web version of this article.)

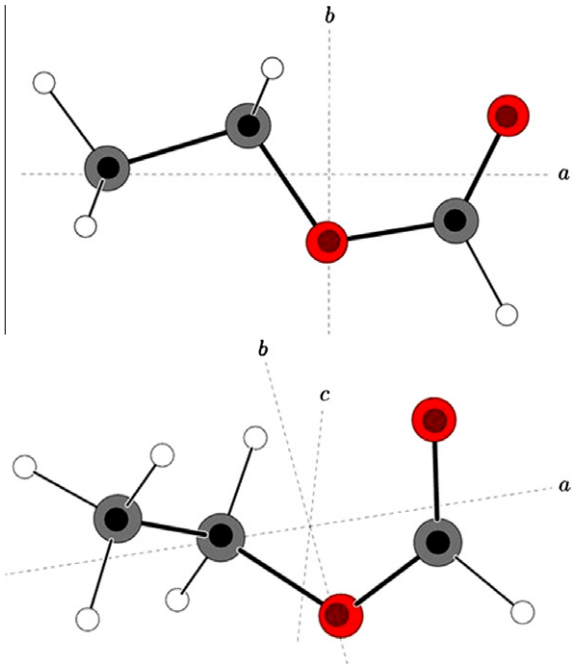

Fig. 8. The Kraitchman substitution structures of *cis–trans* ethyl formate (above) and *cis–gauche* ethyl formate (below). The small spheres represent the experimental positions. The larger spheres are the ab initio positions at MP2/6-311++G(d,p).

Table 6
Kraitchman substitution coordinates of the *cis–trans* conformer of ethyl formate. The uncertainties are Costain errors. The bold-italicized letter indicates the atom coordinate.

	Substitution coordinates[a]		Ab initio coordinates[b]	
	$\|a\|$ (Å)	$\|b\|$ (Å)	a (Å)	b (Å)
$CH_3CH_2O\boldsymbol{C}HO$	1.2996(12)	0.4748(32)	−1.303	0.478
$CH_3\boldsymbol{C}H_2OCHO$	0.8307(18)	0.5001(30)	0.833	−0.498
$\boldsymbol{C}H_3CH_2OCHO$	2.2782(67)	0.0641(23)	2.281	−0.057
$CH_3CH_2OCH\boldsymbol{O}$	1.8365(82)	0.6015(25)	−1.840	−0.604
$CH_3CH_2\boldsymbol{O}CHO$	$\|0\|$[c]	0.6930(22)	0.022	0.690

[a] Principal axis, planar coordinates.
[b] MP2/6-311++G(d,p).
[c] Coordinate constrained to zero.

Table 7
Kraitchman substitution coordinates of the *cis–gauche* conformer of ethyl formate. The uncertainties are Costain errors. The bold-italicized letter indicates the atom coordinate.

	Substitution coordinates[a]			Ab initio coordinates[b]		
	$\|a\|$ (Å)	$\|b\|$ (Å)	$\|c\|$ (Å)	a (Å)	b (Å)	c (Å)
$CH_3CH_2O\boldsymbol{C}HO$	1.2248(12)	0.2494(20)	0.2558(59)	−1.224	0.250	0.255
$\boldsymbol{C}H_3CH_2OCHO$	1.7506(86)	0.6366(24)	0.3400(44)	1.734	−0.646	0.347
$CH_3\boldsymbol{C}H_2OCHO$	0.9850(15)	0.3002(50)	0.5644(27)	0.990	0.319	−0.558
$CH_3CH_2OCH\boldsymbol{O}$	1.4192(11)	0.8523(18)	0.1813(83)	−1.411	−0.855	−0.197
$CH_3CH_2\boldsymbol{O}CHO$	0.056(27)	0.9660(16)	0.141(11)	−0.094	0.968	0.151

[a] Principal axis, non-planar coordinates.
[b] MP2/6-311++G(d,p).

the EVAL program [23], are presented in Tables 6–8. All of the fit isotopologue rotational constants are reported in Tables 9 and 10. The frequencies of the measured transitions can be found in the Supplementary material in Tables S-3 and S-4. An interesting aspect of the ethyl torsional potential of ethyl formate, which was originally noted by Riveros and Wilson [51], is that the rotational constants of the *cis–gauche* conformer suggested that the value of the ethyl dihedral angle of this conformer is not approximately 120° but instead is closer to 90°. Using the direct structural information obtained in this study, we find the value of this dihedral angle to be 97(3)°. The structure of ethyl formate was also investigated by Peng et al. [57] using a combination of gas-phase electron diffraction, the microwave data of Riveros and Wilson, and infrared data with additional input from equilibrium geometries calculated using low-level electronic structure theory. The results from the present study agree with 98.3° ethyl dihedral angle reported by Peng et al. Comparisons of the structures obtained here and those obtained by Peng et al. are found in Fig. 9. The most notable differences can be seen in the carbon atom positions. Consequently, the atom coordinates obtained in this study are in better agreement with high level ab initio calculations. Generally, the three structures (CP-FMTW, Peng et al.,

Table 8
Experimental geometric parameters of the two lowest energy conformers of ethyl formate. Internals were calculated using EVAL [23]. Calculations were performed at the MP2/6-311++G(d,p) level of theory.

Species	Bond	Bond length (Å)	Theory	Peng	Angle	Angle (°)	Theory	Peng
Cis–trans	C═O	1.202(5)	1.208	1.209(2)	O═C—O	126.04(84)	125.83	124.1(1)
	C—O	1.317(1)	1.342	1.350(2)	C—O—C	115.31(31)	114.67	117.3(1)
	O—C	1.453(3)	1.446	1.463(2)	O—C—C	108.08(58)	107.17	105.4(1)
	C—C	1.511(6)	1.512	1.493(2)				
Cis–gauche	C═O	1.201(4)	1.21	1.209(2)	O═C—O	125(2)	126.16	124.4(1)
	C—O	1.37(2)	1.34	1.351(2)	C—O—C	114(1)	115.34	117.8(1)
	O—C	1.42(2)	1.45	1.463(2)	O—C—C	111(1)	111.10	109.7(1)
	C—C	1.510(6)	1.52	1.501(2)				

Table 9
Fit spectral parameters for the isotopologues of *cis–trans* ethyl formate. Distortion has been held to the value of the parent species obtained here.

	$CH_3CH_2O^{13}CHO$	$CH_3{}^{13}CH_2OCHO$	$^{13}CH_3CH_2OCHO$	$CH_3CH_2OCH^{18}O$	$CH_3CH_2{}^{18}OCHO$
A (MHz)	17610.2800(61)	17594.3855(64)	17744.2141(61)	17336.3496(80)	17181.1699(74)
B (MHz)	2877.04178(74)	2893.29581(77)	2821.36677(74)	2798.4043(10)	2904.95800(90)
C (MHz)	2554.43319(66)	2566.94655(69)	2513.18481(68)	2486.65608(89)	2566.98682(91)
N_{lines}	34	32	33	22	25
rms (kHz)	18.2	18.1	17.9	8.7	14.3

Table 10
Fit spectral parameters for the isotopologues of *cis–gauche* ethyl formate. Distortion has been held to the value of the parent species obtained here.

	$CH_3CH_2O^{13}CHO$	$^{13}CH_3CH_2OCHO$	$CH_3{}^{13}CH_2OCHO$	$CH_3CH_2OCH^{18}O$	$CH_3CH_2{}^{18}OCHO$
A (MHz)	9961.1011(31)	9888.2971(27)	9907.1546(24)	9714.4007(33)	9638.6239(44)
B (MHz)	3794.8924(10)	3749.5439(12)	3802.7502(12)	3724.7665(10)	3838.3725(19)
C (MHz)	3181.56125(72)	3144.1105(10)	2191.4905(10)	3107.12698(75)	3176.6777(14)
N_{lines}	27	27	21	17	15
rms (kHz)	21.3	21.4	25.1	27.6	24.8

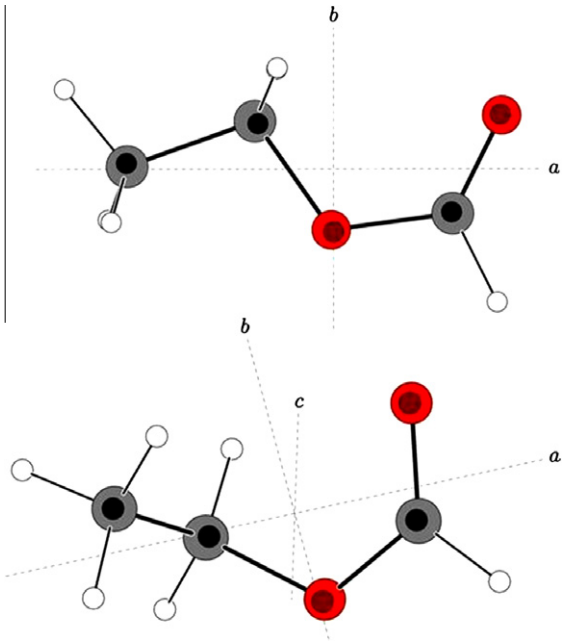

Fig. 9. The Kraitchman substitution structures of *cis–trans* ethyl formate (above) and *cis–gauche* ethyl formate (below). The small spheres represent the experimental positions. The larger spheres are the positions obtained from Peng et al. [57]. The most noticeable differences are in the carbon atom positions.

and ab initio) seem to be in good agreement. The newly determined rotational constants for both normal species conformers of ethyl formate are reported in Table 11. Observed rotational transitions for both conformers of ethyl formate are found in the Supplementary material in Tables S-1 and S-2, and compared to the literature [51] where there is overlap.

4. Discussion of spectrometer design and performance

Broadband spectrometer designs raise new issues in spectrometer performance related to spurious signals, and several measurement issues encountered in this work deserve mention. The original design for the spectrometer microwave electronics used the 23 GHz PDRO to both upconvert the AWG pulse and to downconvert the molecular signals for digitization. This design produced spectral images at about 10% the intensity of the desired spectrum. These images originated from the 23 GHz PDRO undergoing frequency multiplication (to 46 GHz) in the broadband mixer and this frequency acting as a second local oscillator. As a result, two images of the molecular spectrum with LO frequencies of 23 GHz and 46 GHz were observed. An independent 44 GHz PDRO local oscillator was chosen to mix "from above" in the spectrum downconversion to solve this design problem.

Additionally, in the course of this work it became clear that two-tone intermodulation (IM) signals can be a major source of spurious frequencies in the measurement. The spurious signals in question are caused by the molecular emission itself, not spurious signals associated with the digital oscilloscopes, for example. When there are two strong transitions in the spectrum they mod-

Table 11
Fit spectral parameters for *cis–trans* ethyl formate and *cis–gauche* ethyl formate. Two fits are reported, one with distortion obtained from this study (left values), and one with holding the distortion constant to those obtained in [55] (right value).

	Cis–trans ethyl formate		*Cis–gauche* ethyl formate	
A (MHz)	17746.6682(44)	17746.6792(18)	9985.5672(20)	9985.56543(74)
B (MHz)	2904.7291(24)	2904.73074(31)	3839.6023(11)	3839.60159(34)
C (MHz)	2579.1461(26)	2579.14636(32)	3212.8638(11)	3212.86508(33)
ΔJ (kHz)	0.6181(97)		5.935(14)	
ΔJK (kHz)	−3.366(92)		−32.241(44)	
ΔK (kHz)	49.71(41)		78.68(17)	
δJ (kHz)	0.0970(79)		2.0108(70)	
δK (kHz)	–		7.20(18)	
N_{lines}	54	54	94	94
rms (kHz)	20.4	24.9	22.0	22.9

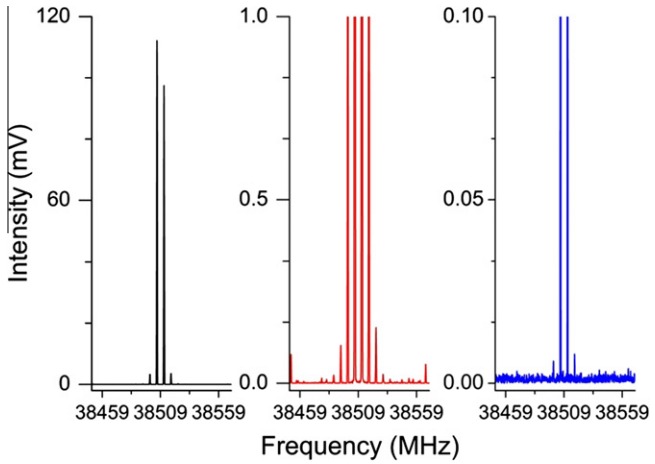

Fig. 10. The black trace shows a portion of the acetaldehyde spectrum (400 000 signal averages) acquired after downconversion. The first modulations can be seen on this scale at about 4 mV. The red trace shows the same portion of the spectrum after 100× magnification, showing the generation of additional sidebands at the two-tone IM frequency. The blue trace (1000 signal averages) is a 40× magnification of acetaldehyde acquired in direct detection on a 100 Gs/s Tektronix oscilloscope. Using the direct detection scheme, which removes the down-conversion mixer from the receiver circuit, the sideband amplitude is significantly reduced and is only about (1/500) of the molecular signals (full transition intensity of 4 mV is off scale in the figure). (For interpretation of the references to color in this figure legend, the reader is referred to the web version of this article.)

ulate the receiver response at their beat frequency and, as a result, sidebands at this beat frequency are imposed on every transition in the spectrum. This effect was especially prominent for the acetaldehyde rotational spectra reported here where the intense, closely spaced A–E transitions produce clearly observed side bands as shown in Fig. 10. The amplitude of the sidebands could be reduced by carefully adjusting the local oscillator power to the mixer. However, this does not remove the effect completely indicating that some of the receiver non-linearity is within the digital oscilloscope.

In a broadband spectrum there are many possible pairs of strong transitions that can create the IM spurs and the direct beat frequencies will appear in a spectral range determined by the frequency bandwidth. For the 25–40 GHz bandwidth of the current spectrometer, beat frequencies up to 15 GHz can be produced by this effect. Therefore, the direct beat signals appear in the measurement frequency range of the downconverted molecular signal (4–19 GHz). These IM spur frequencies can be readily calculated from the spectrum and are, therefore, easily identified. Current digital oscilloscope capabilities can remove this measurement issue by detecting the 25–40 GHz frequency emission directly, removing the need for the broadband downconversion mixing stage. We have tested the spectrometer performance in direct detection using a 100 Gs/s digital oscilloscope (Tektronix DPO73304D with nominal 3 dB hardware bandwidth of 33 GHz but we achieved excellent performance to 40 GHz). A comparison of the direct detection spectrum with the spectrum obtained using broadband signal downconversion is shown in Fig. 11.

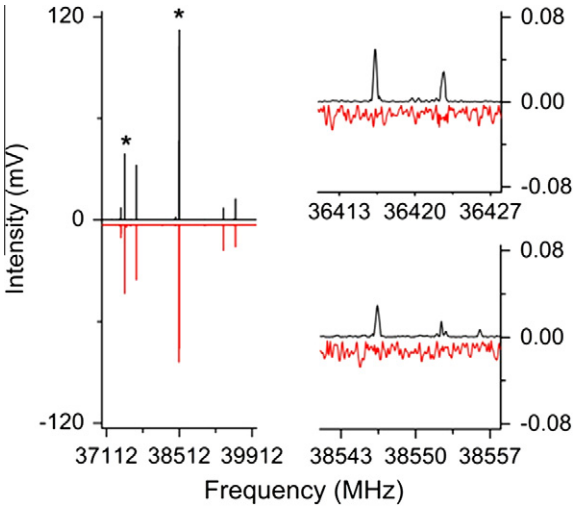

Fig. 11. The black trace is a portion of the acetaldehyde spectrum (400 000 signal averages) acquired after downconverion with a 44 GHz PDRO. The red trace (1000 signal averages, scaled for signal) is acetaldehyde acquired in direct detection on a 100 Gs/s Tektronix oscilloscope. The asterisks highlight strong transitions that generate two-tone IM spur frequencies. On the left is the 2_{12}–1_{11} (A) at 37464.13 MHz and on the right is the pair of transition 2_{02}–1_{01} (E) at 38506.02 MHz and 2_{02}–1_{01} (A) at 38512.08 MHz (these transitions are unresolved at the scale of the figure). These transitions generate two-tone IM spurs at 1041.89 MHz and 1047.95 MHz. The overall gain modulation of the receiver by these beat frequencies places sidebands on other transitions. Shown on the right are the spurious signals resulting from the lower sidebands off the 2_{12}–1_{11} (A) transitions at 37464.13 MHz and the lower sidebands off the 2_{11}–1_{10} (A) transitions at 39594.21 MHz of acetaldehyde. The red trace shows that removal of the downconversion mixer and using direct detection reduces the spur amplitudes in the final spectrum. (For interpretation of the references to color in this figure legend, the reader is referred to the web version of this article.)

5. Conclusions

CP-FTMW spectroscopy in K_a-band is a high-throughput, high-sensitivity extension of chirped-pulse FTMW spectroscopy to an important band for a variety of applications. This is an excellent frequency range for observations of molecules in interstellar clouds, due to frequency overlap with sensitive radio astronomical facilities, both single-dish (GBT) and interferometric (JVLA). Molecular sources such as pulsed discharge nozzles can also be readily incorporated into this spectrometer for the study of terrestrially unstable species or molecules with low volatility. The high phase stability and spectral purity of this instrument allows for deep signal averaging, which allows for low-abundance or low-dipole moment species to be detected.

Acknowledgments

The development of the K_a-band CP-FTMW spectrometer was supported by the Centers for Chemical Innovation program of the National Science Foundation (CHE-0847919).

Appendix A. Supplementary material

Supplementary data for this article are available on ScienceDirect (www.sciencedirect.com) and as part of the Ohio State University Molecular Spectroscopy Archives (http://library.osu.edu/sites/msa/jmsa_hp.htm). Supplementary data associated with this article can be found, in the online version, at http://dx.doi.org/10.1016/j.jms.2012.07.014.

References

[1] G.G. Brown, B.C. Dian, K.O. Douglass, S.M. Geyer, S.T. Shipman, B.H. Pate, Rev. Sci. Instrum. 79 (2008) 053103.
[2] T.J. Balle, W.H. Flygare, Rev. Sci. Instrum. 52 (1981) 33–45.
[3] G.S. Grubbs, C.T. Dewberry, K.C. Etchison, K.E. Kerr, S.A. Cooke, Rev. Sci. Instrum. 78 (2007) 096106.
[4] G.S. Grubbs, S.A. Cooke, J. Mol. Spectrosc. 259 (2009) 120–122.
[5] C.T. Dewberry, Z. Kisiel, S.A. Cooke, J. Mol. Spectrosc. 261 (2010) 82–86.
[6] S.L. Stephens, N.R. Walker, J. Mol. Spectrosc. 263 (2010) 27–33.
[7] A. Lesarri, S.T. Shipman, J.L. Neill, G.G. Brown, R.D. Suenram, L. Kang, W. Caminati, B.H. Pate, J. Am. Chem. Soc. 132 (2010) 13417.
[8] Z. Kisiel, A. Lesarri, J.L. Neill, M.T. Muckle, B.H. Pate, Phys. Chem. Chem. Phys. 13 (2011) 13912–13919.

[9] D.A. Obenchain, A.A. Elliot, A.L. Steber, R.A. Peebles, S.A. Peebles, C.J. Wurrey, G.A. Guirgis, J. Mol. Spectrosc. 261 (2010) 35–40.
[10] R.G. Bird, J.L. Neill, V.J. Alstadt, J.W. Young, B.H. Pate, D.W. Pratt, J. Phys. Chem. A. 115 (2011) 9392.
[11] G.B. Park, A.H. Steeves, K. Kuyanov-Prozument, J.L. Neill, R.W. Field, J. Chem. Phys. 135 (2011) 024202.
[12] K. Prozument, A.P. Colombo, Y. Zhou, G.B. Park, V.S. Petrovíc, S.L. Coy, R.W. Field, Phys. Rev. Lett. 107 (2011) 143001.
[13] E. Gerecht, K.O. Douglass, D.F. Plusquellic, Opt. Exp. 19 (2011) 8973–8984.
[14] National Radio Astronomy Observatory, <http://almascience.nrao.edu/alma-data/science-verification>.
[15] GBT PRebiotic Interstellar MOlecule Survey, <www.cv.nrao.edu/~aremijan/PRIMOS>.
[16] Y. Ohshima, Y. Endo, Chem. Phys. Lett. 256 (1996) 635–640.
[17] C.A. Gottlieb, A.J. Apponi, M.C. McCarthy, P. Thaddeus, J. Chem. Phys. 113 (2000) 1910–1915.
[18] S. Brünken, H. Gupta, C.A. Gottlieb, M.C. McCarthy, P. Thaddeus, Astrophys. J. 644 (2007) L43–L46.
[19] M.C. McCarthy, P. Thaddeus, J.J. Wilke, H.F. Schaefer III, J. Chem. Phys. 130 (2009) 234304.
[20] G.L. Storck, C. Karunatlaka, E.B. Biddle, R. Crawley Jr., K.M. Hotopp, A.J. Shirar, B.C. Dian, J. Phys. Chem. Lett. 1 (2010) 1547–1551.
[21] R.C. Woods, R.J. Saykally, Philos. Trans. Roy. Soc. A 324 (1988) 141–146.
[22] Z. Kisiel, L. Pszczółkoski, I.R. Medvedev, M. Winnewisser, F.C. DeLucia, E. Herbst, J. Mol. Spectrosc. 233 (2005) 231–243.
[23] Z. Kisiel, PROSPE, Programs for ROtational SPEctroscopy. <http://info.ifpan.edu.pl/~kisiel/prospe.htm>.
[24] H.M. Pickett, J. Mol. Spectrosc. 148 (1991) 371–377.
[25] H.M. Pickett, SPFIT/SPCAT Package, <http://spec.jpl.nasa.gov>.
[26] M.J. Frisch, G.W. Trucks, H.B. Schlegel, G.E. Scuseria, M.A. Robb, J.R. Cheeseman, G. Scalmani, V. Barone, B. Mennucci, G.A. Petersson, H. Nakatsuji, M. Caricato, X. Li, H.P. Hratchian, A.F. Izmaylov, J. Bloino, G. Zheng, J.L. Sonnenberg, M. Hada, M. Ehara, K. Toyota, R. Fukuda, J. Hasegawa, M. Ishida, T. Nakajima, Y. Honda, O. Kitao, H. Nakai, T. Vreven, J.A. Montgomery Jr., J.E. Peralta, F. Ogliaro, M. Bearpark, J.J. Heyd, E. Brothers, K.N. Kudin, V.N. Staroverov, R. Kobayashi, J. Normand, K. Raghavachari, A. Rendell, J.C. Burant, S.S. Iyengar, J. Tomasi, M. Cossi, N. Rega, J.M. Millam, M. Klene, J.E. Knox, J.B. Cross, V. Bakken, C. Adamo, J. Jaramillo, R. Gomperts, R.E. Stratmann, O. Yazyev, A.J. Austin, R. Cammi, C. Pomelli, J.W. Ochterski, R.L. Martin, K. Morokuma, V.G. Zakrzewski, G.A. Voth, P. Salvador, J.J. Dannenberg, S. Dapprich, A.D. Daniels, O. Farkas, J.B. Foresman, J.V. Ortiz, J. Cioslowski, D.J. Fox, Gaussian, Inc., Wallingford, CT.
[27] F.J. Lovas, R.D. Suenram, J. Chem. Phys. 87 (1987) 2010–2020.
[28] CDMS H.S.P. Müller, F. Schlöder, J. Stutzki, G. Winnewisser, J. Mol. Struct. 742 (2005) 215–227.
[29] Applied Systems Engineering, Inc., <http://www.applsys.com/>.
[30] I. Kleiner, F.J. Lovas, M. Godefroid, J. Phys. Chem. Ref. Data 25 (1996) 1113–1210.
[31] I. Kleiner, J.C. Lopez, S. Blanco, A.R.W. McKellar, N. Moazzen-Ahmadi, J. Mol. Spectrosc. 197 (1999) 275–288.
[32] L. Martinache, A. Bauder, Chem. Phys. Lett. 6 (1989) 657.
[33] P.H. Turner, P.A. Cox, J.A. Hardy, J. Chem. Soc. Faraday Trans. 77 (1981) 1217–1231.
[34] P.A. Cox, K.H. Houghes, J.N. McDonald, Mol. Phys. 101 (2003) 569–574.
[35] D.W. Knight, P.A. Cox, Th. Pedersen, J. Mol. Struct. 189 (1988) 187–201.
[36] R.W. Kilb, C.C. Lin, E.B. Wilson, J. Chem. Phys. 26 (1957) 1695.
[37] P.H. Turner, P.A. Cox, Chem. Phys. Lett. 42 (1976) 84–88.
[38] B.E. Turner, R. Terzieva, E. Herbst, Acc. Chem. Res. 32 (1999) 334.
[39] H.E. Matthews, P. Friberg, W.M. Irvine, Astrophys. J. 290 (1985) 609.
[40] N. Fourkis, M.W. Sinclair, B.J. Robinson, P.D. Godfrey, R.D. Brown, Aust. J. Phys. 27 (1974) 425.
[41] M.B. Bell, H.E. Matthews, P.A. Feldman, Astron. Astrophys. 127 (1983) 420.
[42] B.E. Turner, Astrophys. J. Suppl. 76 (1991) 617.
[43] L.M. Ziurys, D. McGonagle, Astrophys. J. Suppl. 89 (1993) 155.
[44] A. Nummelin, J.E. Dickens, P. Bergman, Å. Hjalmarson, W.M. Irvine, M. Ikeda, M. Ohishi, Astron. Astrophys. 337 (1998) 275–286.
[45] M. Ikeda, M. Ohishi, A. Nummelin, J.E. Dickens, P. Bergman, Å Hjalmarson, W.M. Irvine, Astrophys. J. 560 (2001) 792.
[46] S.B. Charnley, Adv. Space Res. 33 (2004) 23.
[47] R.T. Garrod, S.L. Widicus Weaver, E. Herbst, Astrophys. J. 682 (2008) 283–302.
[48] W.L. Barclay Jr., M.A. Anderson, L.M. Ziurys, I. Kleiner, J.T. Hougen, Astrophys. J. Suppl. 89 (2003) 221–226.
[49] L. Margulès, R.A. Motiyenko, THz spectroscopy of 13C isotopic species of a "Weed": acetaldehyde, in: The Ohio State 66th International Symposium on Molecular, Spectroscopy, June 24, 2011.
[50] M. Elkeurti, L.H. Coudert, I.R. Medvedev, et al., J. Mol. Spectrosc. 263 (2010) 145.
[51] J.M. Riveros, E.B. Wilson, J. Chem. Phys. 46 (1967) 4605.
[52] R. Meyer, E.B. Wilson, J. Chem. Phys. 53 (1970) 3969.
[53] V.K. Kaushik, Chem. Phys. Lett. 70 (1980) 317–320.
[54] J. Demaison, D. Boucher, J. Burie, A. Dubrulle, Z. Naturforsch. 39A (1984) 560.
[55] I.R. Medvedev, F.C. De Lucia, E. Herbst, Astrophys. J. Suppl. 181 (2009) 433–438.
[56] A. Belloche, R.T. Garrod, H.S.P. Mueller, K.M. Menten, C. Comito, P. Schilke, Astron. Astrophys. 499 (2009) 215.
[57] Z. Peng, S. Shlykov, C. Van Alsenoy, H.J. Geise, B. Van der Veken, J. Chem. Phys. 99 (1995) 10201–10212.